Quantum cascade laser master-oscillator power-amplifier with 1.5 W output power at 300 K

Stefan Menzel,[1] Laurent Diehl,[1,2] Christian Pflügl,[1,2] Anish Goyal,[3] Christine Wang,[3] Antonio Sanchez,[3] George Turner,[3] and Federico Capasso[1,*]

[1] *Harvard University, School of Engineering and Applied Sciences, 29 Oxford St., Cambridge, MA 02138, USA*
[2] *Eos Photonics, Inc., 30 Spinelli Place, Cambridge, MA 02138, USA*
[3] *MIT Lincoln Laboratory, 244 Wood St., Lexington, MA 02420, USA*
[*] *capasso@seas.harvard.edu*

Abstract: We report quantum cascade laser (QCL) master-oscillator power-amplifiers (MOPAs) at 300 K reaching output power of 1.5 W for tapered devices and 0.9 W for untapered devices. The devices display single-longitudinal-mode emission at λ = 7.26 µm and single-transverse-mode emission at TM_{00}. The maximum amplification factor is 12 dB for the tapered devices.

OCIS codes: (140.5965) Semiconductor lasers, quantum cascade; (140.3280) Laser amplifiers.

References and links

1. J. Faist, F. Capasso, D. L. Sivco, C. Sirtori, A. L. Hutchinson, and A. Y. Cho, "Quantum cascade laser," Science **264**(5158), 553–556 (1994).
2. C. Gmachl, F. Capasso, D. L. Sivco, and A. Y. Cho, "Recent progress in quantum cascade lasers and applications," Rep. Prog. Phys. **64**(11), 1533–1601 (2001).
3. A. A. Kosterev and F. K. Tittel, "Chemical sensors based on quantum cascade lasers," IEEE J. Quantum Electron. **38**(6), 582–591 (2002).
4. R. F. Curl, F. Capasso, C. Gmachl, A. A. Kosterev, B. McManus, R. Lewicki, M. Pusharsky, G. Wysocki, and F. K. Tittel, "Quantum cascade lasers in chemical physics," Chem. Phys. Lett. **487**(1-3), 1–18 (2010).
5. C. W. Van Neste, L. R. Senesac, and T. Thundat, "Standoff spectroscopy of surface adsorbed chemicals," Anal. Chem. **81**(5), 1952–1956 (2009).
6. F. Fuchs, S. Hugger, M. Kinzer, R. Aidam, W. Bronner, R. Lösch, Q. Yang, K. Degreif, and F. Schnürer, "Imaging standoff detection of explosives using widely tunable midinfrared quantum cascade lasers," Opt. Eng. **49**(11), 111127 (2010).
7. L. Diehl, C. Pflügl, M. F. Witinski, P. Wang, T. J. Tague, Jr., and F. Capasso, "Fourier transform spectrometers utilizing mid-infrared quantum cascade lasers," Lasers and Electro-Optics/Quantum Electronics and Laser Science Conference: 2010 Laser Science to Photonic Applications, CLEO/QELS 2010, 5500620.
8. Y. Bai, S. Slivken, S. R. Darvish, A. Haddadi, B. Gökden, and M. Razeghi, "High power broad area quantum cascade lasers," Appl. Phys. Lett. **95**(22), 221104 (2009).
9. N. Yu, L. Diehl, E. Cubukcu, D. Bour, S. Corzine, G. Höfler, A. K. Wojcik, K. B. Crozier, A. Belyanin, and F. Capasso, "Coherent coupling of multiple transverse modes in quantum cascade lasers," Phys. Rev. Lett. **102**(1), 013901 (2009).
10. C. S. Kim, M. Kim, W. W. Bewley, J. R. Lindle, C. L. Canedy, J. A. Nolde, D. C. Larrabee, I. Vurgaftman, and J. R. Meyer, "Broad-stripe, single-mode, mid-IR interband cascade laser with photonic-crystal distributed-feedback grating," Appl. Phys. Lett. **92**(7), 071110 (2008).
11. B. Gökden, Y. Bai, N. Bandyopadhyay, S. Slivken, and M. Razeghi, "Broad area photonic crystal distributed feedback quantum cascade lasers emitting 34 W at λ~4.36 µm," Appl. Phys. Lett. **97**(13), 131112 (2010).
12. H. Zhang, A. Seetharaman, P. Johnson, G. Luo, and H. Q. Le, "High-gain low-noise mid-infrared quantum cascade optical preamplifier for receiver," IEEE Photon. Technol. Lett. **17**(1), 13–15 (2005).
13. M. Spreemann, M. Lichtner, M. Radziunas, U. Bandelow, and H. Wenzel, "Measurement and simulation of distributed-feedback tapered master-oscillator power amplifiers," IEEE J. Quantum Electron. **45**(6), 609–616 (2009) (and references therein).
14. H. Wenzel, K. Paschke, O. Brox, F. Bugge, J. Fricke, A. Ginolas, A. Knauer, P. Ressel, and G. Erbert, "10W continuous-wave monolithically integrated master-oscillator power-amplifier," Electron. Lett. **43**(3), 160–162 (2007).
15. M. Troccoli, C. Gmachl, F. Capasso, D. L. Sivco, and A. Y. Cho, "Mid-infrared (λ~7.4 µm) quantum cascade laser amplifier for high power single-mode emission and improved beam quality," Appl. Phys. Lett. **80**(22), 4103 (2002).
16. C. Gmachl, D. L. Sivco, R. Colombelli, F. Capasso, and A. Y. Cho, "Ultra-broadband semiconductor laser," Nature **415**(6874), 883–887 (2002).

#148896 - $15.00 USD Received 7 Jun 2011; revised 21 Jul 2011; accepted 24 Jul 2011; published 9 Aug 2011

17. A. Wittmann, A. Hugi, E. Gini, N. Hoyler, and J. Faist, "Heterogeneous high-performance quantum-cascade laser sources for broad-band tuning," IEEE J. Quantum Electron. **44**(11), 1083–1088 (2008).
18. S. Slivken, A. Evans, W. Zhang, and M. Razeghi, "High-power, continuous-operation intersubband laser for wavelengths greater than 10 μm," Appl. Phys. Lett. **90**(15), 151115 (2007).
19. J. S. Yu, S. Slivken, A. J. Evans, and M. Razeghi, "High-performance continuous-wave operation of λ~4.6 μm quantum-cascade lasers above room temperature," IEEE J. Quantum Electron. **44**(8), 747–754 (2008).
20. R. Maulini, A. Lyakh, A. Tsekoun, R. Go, C. Pflügl, L. Diehl, F. Capasso, and C. K. N. Patel, "High power thermoelectrically cooled and uncooled quantum cascade lasers with optimized reflectivity facet coatings," Appl. Phys. Lett. **95**(15), 151112 (2009).
21. B. G. Lee, M. A. Belkin, C. Pflügl, L. Diehl, H. A. Zhang, R. M. Audet, J. MacArthur, D. P. Bour, S. W. Corzine, G. E. Höfler, and F. Capasso, "DFB quantum cascade laser arrays," IEEE J. Quantum Electron. **45**(5), 554–565 (2009).
22. A. Yariv and P. Yeh, *Photonics: Optical Electronics in Modern Communications*, 6th ed., chapter 16 (Oxford University Press, 2006).
23. A. Wittmann, Y. Bonetti, M. Fischer, J. Faist, S. Blaser, and E. Gini, "Distributed-feedback quantum-cascade lasers at 9 μm operating in continuous wave up to 423 K," IEEE Photon. Technol. Lett. **21**(12), 814–816 (2009).
24. B. Gökden, Y. Bai, S. Tsao, N. Bandyopadhyay, S. Slivken, and M. Razeghi, "High power 1D and 2D photonic crystal distributed feedback quantum cascade lasers," SPIE Proc. **7945**, 79450C, 79450C-12 (2011).
25. Q. Y. Lu, Y. Bai, N. Bandyopadhyay, S. Slivken, and M. Razeghi, "Room-temperature continuous wave operation of distributed feedback quantum cascade lasers with watt-level power output," Appl. Phys. Lett. **97**(23), 231119 (2010).

1. Introduction

Quantum cascade lasers (QCLs) [1,2] are a well-established laser source in the mid-infrared spectral region. Their use in spectroscopic applications has been demonstrated in a variety of experiments [3,4]. QCLs with high output power and single-mode emission are especially well suited for applications such as stand-off detection [5,6] and liquid phase spectroscopy [7] with a high extinction ratio. Achieving high output power while maintaining a single-mode emission spectrum and good beam quality, however, is difficult.

The most straightforward approach is to increase the geometric dimensions of the laser, but simply widening the laser cavity to obtain very broad laser ridges is not viable as it leads to poor beam quality and a multimode spectrum arising from high-order transverse modes [8,9]. The most promising and perhaps most complicated approach to date utilizes broad-area devices with two-dimensional photonic-crystal distributed-feedback (PCDFB) gratings patterned on the side of the waveguide [10]; single-mode interband cascade lasers 400 μm wide with $M^2<2$ were demonstrated up to the highest current achievable although the output power was limited by diffraction losses and a low coupling coefficient. The implementation of this approach in QCLs at longer wavelength has been less successful. Significant progress has been made recently [11] leading to demonstration of broad-area QCLs with peak output power of 34 W at room temperature, but the far field of the device degraded significantly as function of current. High power in QCLs can also be achieved by adjusting the doping in the structure, allowing devices to operate at high current densities and hence high optical gain. This approach, however, is limited by device self-heating, jeopardizing high-performance continuous-wave operation; even in pulsed operation it typically results in a significant broadening of the linewidth of the emission spectrum.

A different way to achieve high-output-power single-mode lasers is by fabrication of a monolithic two-section device, where one section is a DFB laser acting as a seed laser, referred to as master oscillator (MO), and the other section serves as a power amplifier (PA) [12,13]. This approach has been particularly successful with near-infrared diode lasers, and MOPA lasers with continuous wave (CW) power up to 10 W have also been demonstrated [14]. The first proof-of-concept QCL MOPAs were demonstrated by Troccoli et al. [15].

The most attractive features of MOPA lasers are that only standard elements such as a DFB laser are required and that single-mode emission and excellent beam quality are assured as long as the seed DFB laser supports the fundamental TM_{00} mode. Moreover, in MOPA lasers the coupling losses are minimal since the output from the MO couples directly into the PA and the entire device is fabricated on-chip by means of standard semiconductor technology. The output power of the MOPA is determined first by the MO output power and second by the gain coefficient and the length of the PA, which is a single-pass traveling-wave

#148896 - $15.00 USD Received 7 Jun 2011; revised 21 Jul 2011; accepted 24 Jul 2011; published 9 Aug 2011

amplifier. Tapering the PA allows higher-power amplification prior to reaching possible gain saturation. Also the far-field angle in the chip plane is reduced by the larger PA facet.

A technological challenge for MOPA devices is suppression of self-lasing of the PA. Previous efforts in MOPA QCLs used an end facet cleaved at an angle to prevent the PA cavity from self-lasing. The deposition of antireflection (AR) coatings is a more controllable and efficient way to suppress self-lasing, and the PA facet reflectivity can be reduced to <0.001 by the choice of suitable materials and number of layers. A very low reflectivity allows the end facet to remain orthogonal to the light propagation direction. This results in a better beam quality and lower power losses than with an uncoated angled facet, which relies on the principle of directing light toward the ridge sidewalls, instead of directly reducing the reflectivity.

In this paper we report MOPA QCL devices emitting peak output power of 1.5 W at 300 K with single-mode emission at $\lambda = 7.26$ µm. The devices have a low-reflectivity AR coating applied to the PA end facet. Devices with untapered and tapered PAs were fabricated.

2. Materials and fabrication

The QCL active region material was grown by metalorganic vapor-phase epitaxy (MOVPE) on a conducting InP substrate. To enable future use of the QCL material for multiple-wavelength MOPA arrays, we used a graded-active-region design following closely the broadband design reported in Ref [16]. This design does not allow for high output power because each cascaded active region has a lasing transition at a slightly different wavelength, but it provides a broad gain spectrum.

The MOVPE layer sequence starting from the substrate was 4 µm of InP (Si doped, $n = 1 \times 10^{17}cm^{-3}$) followed by 0.8 µm of InGaAs (Si doped, $n = 1 \times 10^{16}cm^{-3}$), both layers serving as the lower waveguide cladding. The graded active region was a slightly modified version of that in Ref. 16. Modifications included changes in quantum-well thicknesses of each cascaded active region to shift the gain to approximately $\lambda_{center} = 7.3$ µm. The layer sequences for the first and last active region/injector are as follows: (in Ångstrom, barrier layers in bold) 33 **20** 32 **21** 30 **23** 29 **24** 28 **24** 27 **42** 18 **13** 60 **14** 48 **20** (λ_{first} ~6.5 µm) and 36 **18** 35 **19** 35 **19** 34 **20** 34 **41** 22 **12** 67 **13** 52 **20** (λ_{last} ~8µm). A chirp in emission wavelength for the intermediate sequences was then applied similar to Ref. 16.

The structure was subsequently capped with 500 nm of InGaAs (Si doped, $n = 1 \times 10^{16}cm^{-3}$), 4.0 µm of InP (Si doped, $n = 1 \times 10^{17}cm^{-3}$), 0.5 µm of InP (Si doped, $n = 5 \times 10^{18}cm^{-3}$) and 20 nm of InGaAs (Si doped, $n = 1 \times 10^{19}cm^{-3}$), which served as the upper waveguide cladding and top contact layers, respectively.

The DFB grating was fabricated by defining the grating structure in the top InGaAs by electron-beam lithography and reactive-ion etching (~250 nm grating depth). The upper InP waveguide layers were then regrown by MOVPE resulting in a buried-grating structure. After regrowth, the MOPA structure was fabricated using standard contact lithography and wet etching (DI water/HBr/bromide water) for ridge definition (15 µm ridge width). Devices with no taper angle in the PA section and a taper angle of 1° were fabricated in addition to Fabry-Perot lasers with different lengths. Electrical insulation was achieved by a 450 nm-thick SiN layer with an opening on top of the ridges, and Ti/Au was used for top and bottom metallization. A metallization gap of 100 µm was used between the PA and the MO sections to allow independent pumping. The devices were cleaved to a length of 2.5 mm (1 mm MO, 1.5 mm PA). The PA end facet was AR coated with a two-layer structure based on ZnS (833 nm) / MgF_2 (1516 nm) incorporating a thin layer of Y_2O_3 (10 nm) to facilitate adhesion of ZnS to the laser facet. Based on this design, the calculated modal reflectivity is <0.1% over a $\Delta\lambda = 1$ µm bandwidth centered around $\lambda = 7.3$ µm. The devices were then mounted epilayer up with indium solder on copper heat sinks for characterization.

#148896 - $15.00 USD Received 7 Jun 2011; revised 21 Jul 2011; accepted 24 Jul 2011; published 9 Aug 2011

3. Measurements

All measurements were performed at T = 300 K under pulsed conditions (20 kHz / 100 ns) using a calibrated thermopile detector for output power measurements.

Spectra of the fabricated MOPA device with a PA taper angle of 1° are shown in Fig. 1. The single-mode emission wavelength λ is 7.26 μm. A side-mode suppression ratio >20 dB is measured and preserved at all pumping currents for both MO and PA. The full width at half-maximum (FWHM) of $\Delta k = 1\ cm^{-1}$ is due to self-heating during the current pulse and does not broaden with higher PA currents. The inset shows a schematic of the device structure for a tapered MOPA QCL, where the mode adiabatically spreads in the PA section and is amplified.

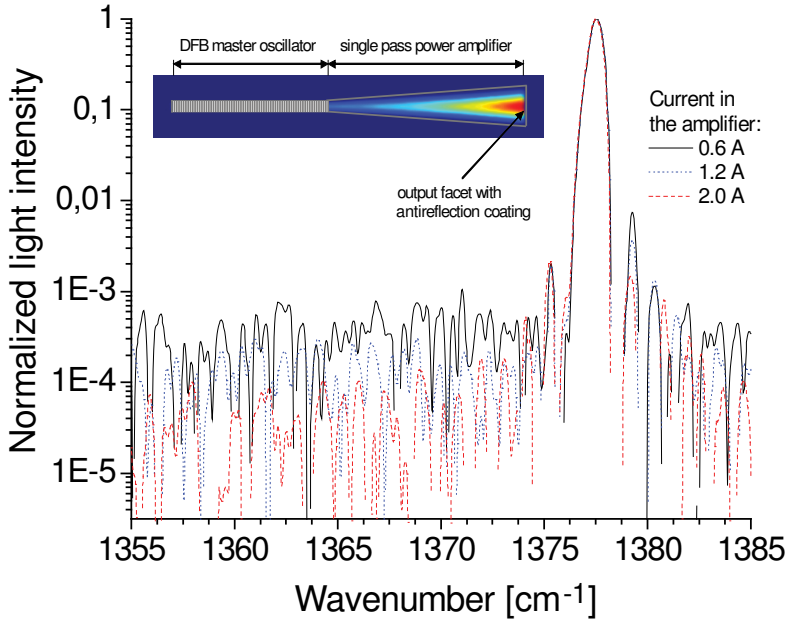

Fig. 1. Spectra of a MOPA with 1° tapered amplifier. The DFB section is kept at 900 mA. The inset shows an illustration of a MOPA device. The light intensity distribution (false colors) has been calculated using a finite-difference time-domain technique. The device geometry is indicated by grey lines. The DFB laser acts as the seed laser while the tapered section is a single-pass traveling wave amplifier.

Figure 2a shows the dependence of the peak output power of the MOPA devices on the MO and PA pumping currents at 300 K, and Fig. 2b shows light-current (L-I) characteristics of a tapered amplifier and untapered amplifier on a current-density scale. In Fig. 2a, the device with no taper angle reaches a peak power P_{out}~900 mW for a MO current I_{MO} = 900 mA corresponding to the rollover point of the L-I characteristic. Devices with 1° taper angle displayed higher peak output power with a maximum P_{out} = 1.5 W, which corresponds to an average power P_{av} = 3 mW for a duty cycle of 0.2%. To estimate the amplification through the amplifier section one needs to know the power input from the MO section into the amplifier. This can be deduced from the data in Fig. 2 if the transparency current density j_{trans} is known. Transparency current is defined as the minimum current where population inversion is reached and light is transmitted without being damped or amplified [17–20]. One method to determine this parameter is to use the dependence of the threshold current j_{th} and the slope efficiency versus cavity length as explained in detail in Ref [20]. In our case, we processed Fabry-Perot QCLs from the same material used for the MOPAs but did not observe a clear dependence of the slope efficiency on the cavity length, especially for short lasers, to determine j_{trans}.

#148896 - $15.00 USD Received 7 Jun 2011; revised 21 Jul 2011; accepted 24 Jul 2011; published 9 Aug 2011

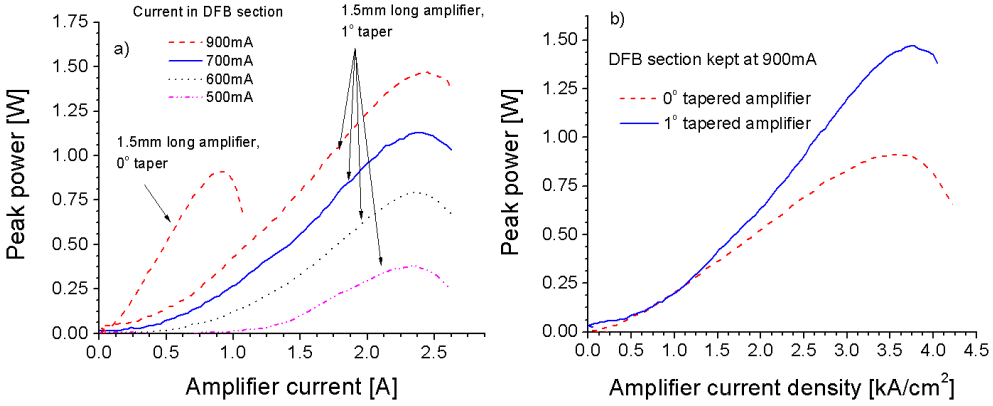

Fig. 2. a) L-I characteristics for different currents in the MO DFB section at T = 300 K. b) Comparison of characteristics for two MOPAs with tapered and untapered PAs on a current-density scale.

Instead, we use the value of the threshold current density for 3mm long Fabry-Perot lasers (j_{th}~1.75 kA/cm^2, see Fig. 3) and the relation

$$j_{th} = \frac{\alpha_w + \alpha_m}{\Gamma g} + j_{trans}, \tag{1}$$

where α_w is the waveguide loss (cm^{-1}), g is the gain coefficient (cm/kA), Γ is the mode confinement factor and α_m is the mirror loss (α_m as in Ref. 19).

In order to estimate the value of j_{trans}, we calculated $g \cdot \Gamma$ = 8.25 cm/kA according to Ref [2], waveguide losses α_w~5.5 cm^{-1} using the commercial software COMSOL Multiphysics in conjunction with Drude model based absorption coefficients for the individual waveguide cladding layers (resulting in a modal refractive index of $\tilde{n}$ = 3.2 + 0.0007i and Γ = 0.55), and for a 3 mm long ridge mirror losses α_m = 4.18 cm^{-1}. Solving Eq. (1) yields j_{trans}~0.55 kA/cm^2. This estimate is in reasonable agreement with the values found in the literature, although it is difficult to compare j_{trans} for different QCL designs and doping levels.

From the data shown in Fig. 2b for the tapered device and assuming a transparency current density of 0.55 kA/cm^2, we find a transmitted light intensity $P_t = P(j = j_{trans})$~90 mW for a MO current of 900 mA, resulting in an amplification factor as high as 16.6, equivalent to ~12 dB, at the rollover point.

In Fig. 2b, the linear dependence of the untapered MOPA output power on the amplifier current is strong evidence that the gain in the PA is saturated. The tapered MOPA output power instead displays a super-linear dependence, with an exponential growth up to ~1.5 kA/cm^2 and a linear dependence at higher current densities up to ~3 kA/cm^2; beyond this point the L-I curve becomes sublinear and eventually rolls over because of the decreasing tunnel coupling between the injector ground state and the upper laser level, a behavior typical of QCLs.

Above the transparency current density j_{trans}, the amplification of the light emitted from the MO section in the PA can be written as

$$P_{out} = P_{in} \cdot e^{[(-\alpha_w + g \cdot \Gamma \cdot (j - j_{trans})) \cdot d]}, \tag{2}$$

where j is the current density (kA/cm^2), d is the amplifier length, and P_{in} is the input power from the MO.

Equation (2) can be rewritten as

$$P_{out} = P_{in} \cdot e^{-\alpha_w \cdot d} \cdot e^{g \cdot \Gamma \cdot (j - j_{trans}) \cdot d} = P_t \cdot e^{g \cdot \Gamma \cdot (j - j_{trans}) \cdot d} \tag{3}$$

#148896 - $15.00 USD Received 7 Jun 2011; revised 21 Jul 2011; accepted 24 Jul 2011; published 9 Aug 2011

Fitting the exponential growth of the optical power of the tapered device (Fig. 2b) above j_{trans} with Eq. (3) allows extraction of the modal gain coefficient $g \cdot \Gamma$ if the transparency current density is known.

Assuming the transparency current density j_{trans} = 0.55 kA/cm^2 and with $P_t(j = j_{trans})$ = 0.09 W, we deduce $g \cdot \Gamma$ = 10.5 cm/kA for a MO current of 900 mA, which is in good agreement with our calculations. Note that varying j_{trans} does not change significantly the value of $g \cdot \Gamma$ deduced from the fit. By assuming a gain of 10.5 cm/kA, which is close to the value calculated and found by fitting data, the amplification factor assuming no saturation $e^{-\alpha_w \cdot d} \cdot e^{g \cdot \Gamma \cdot (j - j_{trans}) \cdot d}$ reaches 49.

A critical factor in predicting the MOPA output power is the MO power P_{in} injected into the PA for amplification. Since the MO is a DFB laser, the output power from both laser end facets relative to each other depends strongly on the cleaved end facet position and can vary depending on whether the DFB section ends with a higher or lower effective refractive index element. The reason for this effect is a variation of the electromagnetic field distribution along the grating, depending on the DFB end facet position with respect to the DFB grating [21]. To eliminate this uncertainty, future devices will include an AR coating on the MO end facet, in addition to a quarter-wavelength shift [22] incorporated into the DFB grating. The AR coating reduces the end facet feedback resulting in a symmetric electromagnetic field distribution along the grating. Quarter-wavelength shifts are primarily used to ensure single-mode emission but can also be used to displace the center of the intensity distribution along the DFB grating closer to the PA, thus increasing P_{in}.

Comparing P_{out} with typical peak output powers from Fabry-Perot ridge lasers fabricated from the same wafer (2.2 W; 3-mm ridge length, 15-µm ridge width), as presented in Fig. 3, shows that the MOPA device operating on a single-longitudinal mode is capable of achieving similar output power as a multimode Fabry-Perot device of comparable volume. Previous MOPA QCL work reported peak output powers at 300 K of 0.25 W at a wavelength λ = 7.5 µm [15]. Recently reported DFB lasers based on a two-phonon active region design reached CW output power of 70 mW for a wavelength λ = 9.0 µm at 300 K [23] utilizing comprehensive thermal management and a high-reflective coating on the back facet. Even higher CW output power was reported for shorter wavelengths (λ~4.8 µm) [24,25], although a strong degradation of the far-field quality was observed. Combining the MOPA design with such a DFB laser optimized for high-power operation could result in an output power >1 W in CW operation. It is worth mentioning that the use of a long DFB QCL to achieve such a high power level would lead to operation on two longitudinal modes, since the long grating will produce strong coupling [23], unless the grating coupling strength is reduced.

Figure 4 shows far-field measurements in the plane of the chip measured at different PA currents. Measurements of FWHM are narrower for tapered devices than for untapered devices by a factor of 3 (1° taper angle, ~10° FWHM; untapered, ~30° FWHM). The PA end facet widths for untapered and 1° tapered devices are 15 µm and 47 µm, respectively, in good agreement with the FWHM reduction. Theoretical values for the diffraction half-angles θ (FWHM = $2 \cdot \theta$) can be estimated for comparison from $\theta = 2 \cdot \lambda / \pi \cdot w$ (e.g., see Ref [22].) and are $\theta_{untapered}$ = 17.6° and $\theta_{tapered}$ = 5.6° for λ = 7.26 µm. Therefore, the theoretical and measured divergences are in good agreement, indicating adiabatic expansion of the optical mode within the tapered PA. This is important for the integration of QCL MOPAs into optical systems.

4. Summary

We report QCL MOPAs reaching output power levels of 1.5 W at room temperature corresponding to an amplifier gain of 12 dB. Single-transverse-mode emission with a FWHM angle of 10° for a taper angle of 1° was measured, and the devices showed single-longitudinal-mode lasing at λ = 7.26 µm.

#148896 - $15.00 USD Received 7 Jun 2011; revised 21 Jul 2011; accepted 24 Jul 2011; published 9 Aug 2011

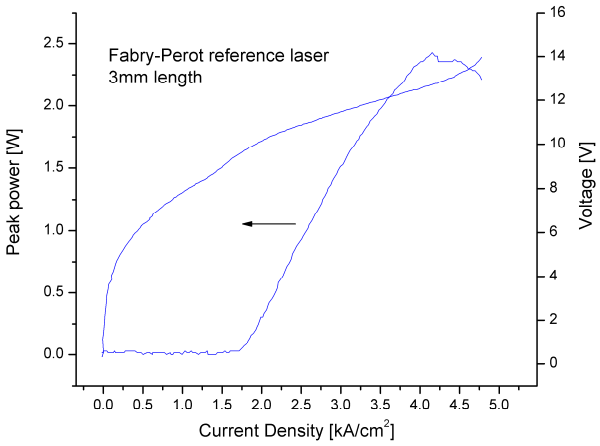

Fig. 3. Light-Current-Voltage characteristic for a 3mm long Fabry-Perot cavity device fabricated from the same wafer as the QCL MOPA devices.

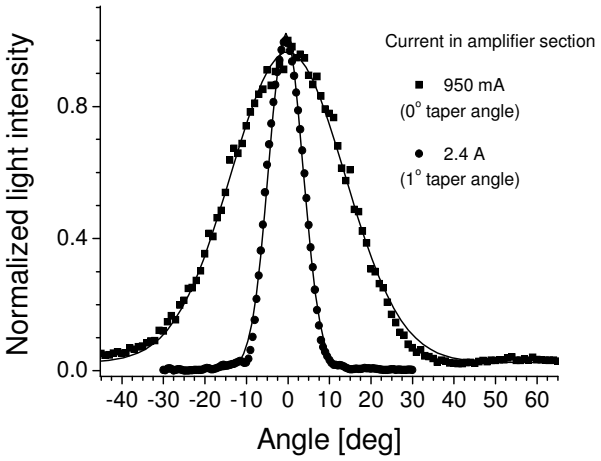

Fig. 4. Far-field measurements in the chip plane for two different taper angles. The PA facet widths are 15 μm (untapered) and 47 μm (1° taper angle). The master oscillator DFB section current is close to rollover (860 mA). Solid lines represent Gaussian fitting curves.

Acknowledgements

The wafers were grown by D. Bour, formerly with Agilent Technologies. The authors acknowledge the Center for Nanoscale Systems (CNS) at Harvard University. Harvard CNS is a member of the National Nanotechnology Infrastructure Network (NNIN). This project received support from the Defense Threat Reduction Agency-Joint Science and Technology Office for Chemical and Biological Defense (Grant no. HDTRA1-10-1-0031-DOD). The Lincoln Laboratory portion of this work was sponsored by the Department of the Air Force under Air Force contract number FA8721-05-C-0002.

#148896 - $15.00 USD Received 7 Jun 2011; revised 21 Jul 2011; accepted 24 Jul 2011; published 9 Aug 2011